Chapter 2

Palette of fluorinated voltage-sensitive hemicyanine dyes

Publication

Chapter 2 of this thesis has been published as: Yan P, Acker* CD, Zhou* WL, Lee* P, Bollensdorff* C, Negrean* A, Lotti* J, Sacconi* L, Antic SD, Kohl P, Mansvelder HD, Pavone FS, Loew LM. (2012) Palette of fluorinated voltage-sensitive hemicyanine dyes. Proc Natl Acad Sci U S A. 2012 109(50):20443-8.

*equal contribution.

Author contributions

P.Y., C.D.A., P.L., C.B., A.N., L.S., S.D.A., P.K., H.D.M., F.S.P., and L.M.L. designed research; P.Y., C.D.A., W.L.Z., P.L., C.B., A.N., J.L., and L.S. performed research; P.Y. contributed new reagents/analytic tools; P.Y., C.D.A., W.L.Z., P.L., C.B., A.N., J.L., L.S., S.D.A., P.K., H.D.M., F.S.P., and L.M.L. analyzed data; and P.L., C.B., A.N., L.S., P.K., and L.M.L. wrote the paper.

2.1 Introduction

Optical recording of membrane potential permits spatially resolved measurement of electrical activity in subcellular regions of single cells, which would be inaccessible to electrodes, and imaging of spatiotemporal patterns of action potential propagation in excitable tissues, such as the brain or heart. However, the available voltage-sensitive dyes (VSDs) are not always spectrally compatible with newly available optical technologies for sensing or manipulating the physiological state of a system. Here, we describe a series of 19 fluorinated VSDs based on the hemicyanine class of chromophores. Strategic placement of the fluorine atoms on the chromophores can result in either blue or red shifts in the absorbance and emission spectra. The range of one-photon excitation wavelengths afforded by these new VSDs spans 440–670 nm; the two-photon excitation

range is 900–1340 nm. The emission of each VSD is shifted by at least 100 nm to the red of its one-photon excitation spectrum. The set of VSDs, thus, affords an extended toolkit for optical recording to match a broad range of experimental requirements. We show the sensitivity to voltage and the photostability of the new VSDs in a series of experimental preparations ranging in scale from single dendritic spines to whole heart. Among the advances shown in these applications are simultaneous recording of voltage and calcium in single dendritic spines and optical electrophysiology recordings using two-photon excitation above 1100 nm.

Optical recording techniques provide powerful tools for neurobiologists [1] and cardiac physiologists [2] to study detailed patterns of electrical activity over time and space in cells, tissues, and organs. Rational design methods, based on molecular orbital calculations of the dye chromophores and characterization of their binding and orientations in membranes [3–5], were used to engineer dye structures. The general class of dye chromophores called hemicyanine (also referred to as styryl dyes) has emerged from this effort as a good foundation for voltage-sensitive dyes (VSDs), because they exhibit electrochromism. This mechanism, also referred to as the molecular Stark effect, involves the differential interaction of the electric field in the membrane with the ground and excited states of the dye chromophore. Several important hemicyanine dyes were produced over the years, including di-4-ANEPPS [6, 7], di-8-ANEPPS [8], di-2-ANEPEQ (also known as JPW-1114) [9, 10], RH-421 and RH-795 [11], ANNINE-6 and ANNINE-6+ [12, 13], di-3-ANEPPDHQ [14, 15], di-4-ANBDQBS, and di-4-ANBDQPQ [16, 17]. Because the electrochromic mechanism is a direct interaction of the electric field with the chromophore and does not require any movement of the dye molecule, all of these dyes provide rapid absorbance and fluorescence responses to membrane potential (V_m); they are, therefore, capable of recording action potentials (APs). Other mechanisms can give more sensitive voltage responses in specialized applications [18–22]. Additionally, new fluorescent protein-based voltage sensors are being developed [23–26], with the promise of being able to genetically target specific cells in an organism. However, to date, hemicyanine dyes are the most universally used and applicable VSDs available. Indeed, among the most recent new advances enabled by these dyes, there has been recording of deep aberrant activity patterns in human hearts from transplant patients [27, 28] and recording V_m spikes ($\approx$1 ms) from individual dendritic spines [29–31].

In this work, we combine instrumentation and experimental protocols to characterize fluorinated hemicyanine VSDs. They are shown in voltage-sensing applications in cardiac and neuronal systems. These systems include random access two-photon imaging of AP propagation in cerebellum; two-photon recording of back-propagating APs (bAPs) from individual dendritic spines in mouse cortical brain slices; tests of long-wavelength two-photon voltage sensing in cultured hippocampal neurons; single-sweep one-photon imaging of dendritic bAPs in cortical neurons; and multiwavelength imaging of V_m and intracellular free calcium ($[Ca^{2+}]_i$) in whole perfused guinea pig heart. These applications are enabled by a series of fluorinated hemicyanine dyes that collectively sample a broad spectral range. Appropriate placement of the fluorine substituents on the dye chromophore allows the excitation and emission spectra of the dyes to be finely tuned. This tuning permits one to choose dyes for optimal sensitivity in relation to the linear or nonlinear excitation sources appropriate to the experimental system as well as minimization of spectral overlap with other fluorescent sensors or optical manipulations. Furthermore, fluorination is known to enhance the

photostability of dye chromophores [32, 33]. For measurements that may be limited by low-dye copy numbers in small volumes and/or the need to record rapid transients, better photostability permits the collection of more photons per VSD molecule, thus improving the signal to noise ratio (S:N) of the optically recorded voltage activity.

2.2 Results

2.2.1 Fluorinated Hemicyanine VSDs

We have synthesized a series of 19 VSDs with various fluorine substitution patterns on three hemicyanine backbone chromophores. The resulting VSDs are shown in Table 2.1 along with their spectral data when bound to the lipid membranes of sonicated soybean phosphatidylcholine vesicles. Also, Table 2.1 shows the corresponding unsubstituted dyes for comparison. The hemicyanine dye chromophores are composed of an electron-donating aromatic amine, a π-linker region, and a heterocyclic electron acceptor [17]. The central portions of the names in Table 2.1 comprise a short code for identifying the structure of the chromophore. The donor moiety for all of these VSDs is 6-amino-naphth-2-yl (AN in the name of the VSD); the linker group is either ethene (E) or a butadiene (BD), and the acceptor is either pyridinium (P) or quinolinium (Q). Thus, the first chromophore in Table 2.1 has an ANEP chromophore (aminonaphthyl ethene pyridinium). A pair of alkyl groups on the amino end anchors the VSD to the membrane, each having two, three, or four carbons that are identified by the prefixes as di-2-, di-3-, or di-4-, respectively. The positions of fluorine substituents are identified by (F), (F2), or (CF3) placed immediately after the moiety on which the substituent has been placed. Finally, all of these VSDs have a 1-prop-3-yl (triethylammonium) head group to impart water solubility and inhibit dye flipping across the membrane; this group is designated by the suffix PTEA.

Table 2.1: Fluorinated VSDs.

Name	Structure	Membrane Abs/Em maxima (nm)	Ethanol solution
Di-n-AN(CF3)EPPTEA (n = 2, 3, 4)	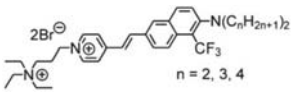	400/589 (n = 2) 411/595 (n = 3) 418/597 (n = 4)	
Di-4-AN(CF3)E(F)PPTEA	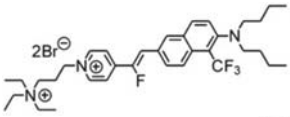	422/590	
Di-4-AN(CF3)EP(F2)PPTEA	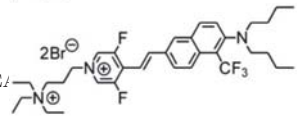	436/608	
Di-n-AN(F)EPPTEA (n = 2, 4)	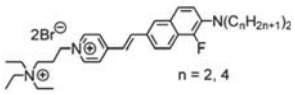	453/616 (n = 2) 444/610 (n = 4)	

Table 2.1 – continued

Name	Structure	Membrane Abs/Em maxima (nm)	Ethanol solution
Di-4-AN(F)E(F)PPTEA	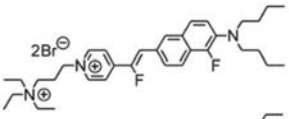	464/643	
Di-4-AN(F)EP(F)PTEA	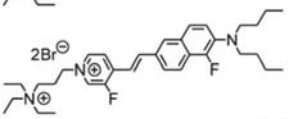	465/632	
Di-4-AN(F)E(F)P(F)PTEA	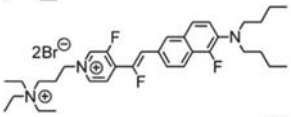	470/651	
Di-4-ANEPPTEA	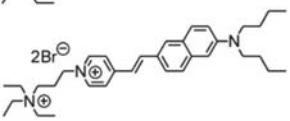	476/616	
Di-n-ANE(F)PPTEA (n = 2, 4)	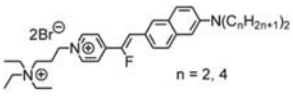	495/642 (n = 2) 488/636 (n = 4)	
Di-n-ANEP(F)PTEA (n = 2, 4)	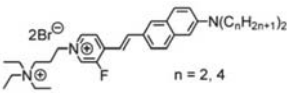	489/632 (n = 2) 495/632 (n = 4)	
Di-4-ANE(F)P(F)PTEA	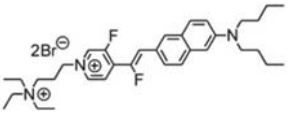	500/660	
Di-n-ANEP(F2)PTEA (n = 2, 4)	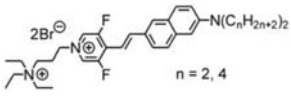	509/648 (n = 2) 511/646 (n = 4)	
Di-2-ANEQPTEA	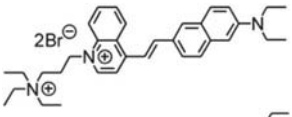	534/664	
Di-4-ANEQ(F)PTEA	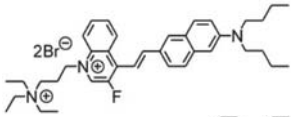	547/686	
Di-2-ANBDQPTEA	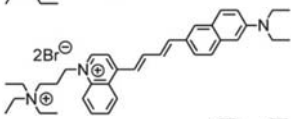	542/702	
Di-2-ANBDQ(F)PTEA	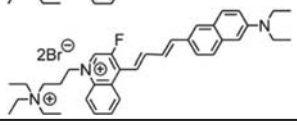	553/743	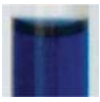

As can be seen, substitution of fluorine at the aminonaphthyl end of the chromophore results in blue shifts of the emission and absorbance spectra; fluorine substitution

within the linker region or the heterocyclic rings (i.e., pyridinium or quinolinium) results in significant red shifts of the spectra. In general, we have prepared both N,N-diethylamino- and N,N-dibutylamino- VSDs. VSDs with n = 2 are more water-soluble, which improves tissue penetration or intracellular spread from a pipette. VSDs with n = 4 are more tightly bound to cell membranes and therefore, more persistent in long-term experiments. All of these VSDs are essentially nonfluorescent in aqueous solution but highly fluorescent when bound to lipid membranes. They have Stokes shifts (difference between the absorbance and emission wavelength maxima) of >150 nm, facilitating their use combined with other fluorescent probes. Also, as detailed in the example applications below, fluorination imparts more photostability than previous generations of hemicyanine dyes. Most important, of course, is their sensitivity to fast voltage changes, which will also be shown by diverse sample applications below.

2.2.2 Recording bAPs from Individual Dendrites and Spines in a Cortical Brain Slice

To optimize the voltage sensitivity of the fluorescent signal ($\Delta F/F$), it is important to excite the hemicyanine dyes at the edge of their spectra, where the change in fluorescence (ΔF) is large but baseline (F) is low [13, 34]. The mode-locked Ti-Sapphire lasers most commonly used for two-photon excitation can be readily tuned up to ca. 1060 nm, but tuning to higher wavelengths, which would be optimal for the nonfluorinated ANEP dyes, results in a rapid decline in laser power. Mode-locked single-wavelength fiber lasers are less costly than tunable Ti-Sapphire lasers and available for excitation at 1064 nm [35]. Therefore, our first syntheses of fluorinated dyes aimed to tune the dye absorbance spectra to place 1060 nm at the red edge. This tuning produced di-2-AN(F)EPPTEA and di-4-AN(F)EPPTEA, VSDs with fluorine substitution on the naphthalene to elicit a blue shift; these dyes are the only dyes in Table 2.1 that have been previously reported [29, 36]. The initial report using di-2-AN(F)EPPTEA was able to show high-quality recordings of bAP from single dendritic spines on a dye-filled pyramidal neuron in a mouse brain slice [29]. In Figure 2.1, we extend this demonstration with a two-photon excited fluorescence record of 5 bAPs evoked by repeated current injection at the soma. Using 1060-nm two-photon excitation, we observe optical bAP waveforms with amplitudes in excess of 17% change in fluorescence. To capture the entire spike train, an extended recording duration of 160 ms was used. Figure 2.1 shows optical recording can follow rapid, repeated AP firing in spines. Additionally, V_m responses to hyperpolarizing current injections can be recorded in a single spine.

It is important to emphasize, however, that the wavelength dependence of $\Delta F/F$ is shallow, which allows some flexibility in the choice of excitation wavelength in response to special experimental demands. We sought to simultaneously record voltage and $[Ca^{2+}]_i$ in single spines by using di-2-AN(F)EPPTEA combined with a fluorescent calcium indicator. This combination was achieved with Calcium Green-1 (conjugated to 3-kDa dextran), which has a one-photon absorbance maximum at 506 nm and emission at 531 nm. The results are shown in Figure 2.2. We chose 1020-nm excitation to excite both fluorescent indicators simultaneously. Xanthene dyes such as Calcium Green have their best two-photon absorbance cross-section into the second electronic excited state at about 800 nm; we reasoned, however, that we could achieve sufficient two-photon excitation directly into the lowest excited state at 1020 nm, which would

allow for simultaneous voltage-sensitive excitation of di-4-AN(F)EPPTEA. The large Stokes shift of the VSD permitted us to readily separate the $[Ca^{2+}]_i$ and voltage signals with appropriate emission filters. Figure 2.2 shows a characteristically slower time course for onset and recovery of the calcium response to bAPs compared with the directly measure optical bAP. Although the $\Delta F/F$ for the VSD is somewhat diminished at 1020 nm (15% compared with 17% at 1060 nm in Figure 2.1), the S:N of the measurement is still sufficient to readily detect a bAP in a single sweep. Thus we achieved a simultaneous recording of voltage and $[Ca^{2+}]_i$ in dendritic spines.

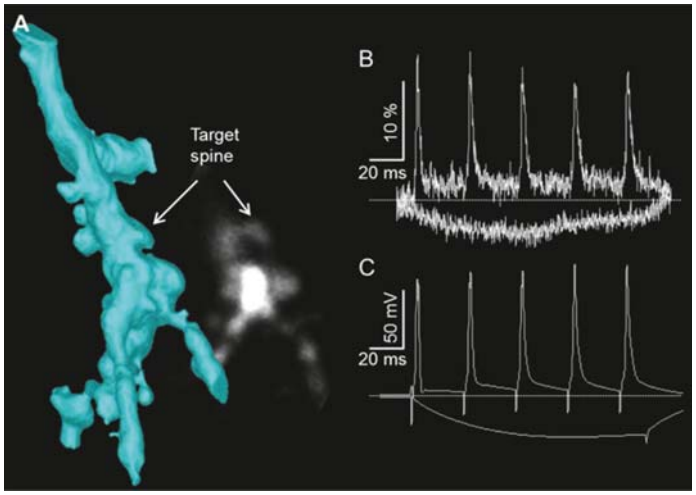

Figure 2.1: AP trains recorded optically in a single dendritic spine. **A)** Reconstruction of the section of basal dendrite showing targeted spine, which looks mushroom-like in the imaging plane (background gray-scale image shows a z-projection spanning 0.5 μm above and below the recording focal plane), but it is clearly stumpy when viewed in the 3D reconstruction. **B)** di-2-AN(F)EPPTEA VSD fluorescence signals recorded from target spine while either five APs were elicited by somatic current pulses or a 150-pA somatic hyperpolarizing current was injected. Total optical recording duration was 160 ms, with 30-ms intervals between APs. Bleaching observed was minimal, and exponential with 1.5-s time constant was subtracted. Waveforms are averages of 40 trials. Excitation wavelength = 1060 nm. **C)** Average of corresponding electrical sweeps.

In Figure 2.3, we use one-photon excitation with a sensitive fast camera to show the ability of two longer-wavelength fluorinated VSDs to record bAPs in dendritic segments of cortical pyramidal neurons; di-2-ANEP(F)PTEA and di-2-ANEP(F2)PTEA have single and double substitutions, respectively, of fluorine at the pyridinium heterocycle to produce a red shift of the hemicyanine chromophore. As above, these dyes were applied intracellularly through a patch pipette, and therefore, they required high solubility in aqueous solution. For both VSDs, the results in Figure 2.3 were obtained with excitation centered at 510 nm. As can be seen, the $\Delta F/F$ for both of these experiments is significantly lower than the spine recording in Figure 2.1 or Figure 2.2. This finding is not likely to be caused by significantly lower sensitivity of these dyes. Rather, lower $\Delta F/F$ can be attributed to a higher total fluorescence caused by internal membrane staining in dendrites compared with spines as previously reported [29]; $\Delta F/F$ would also be greater if the excitation wavelength was shifted farther to the red

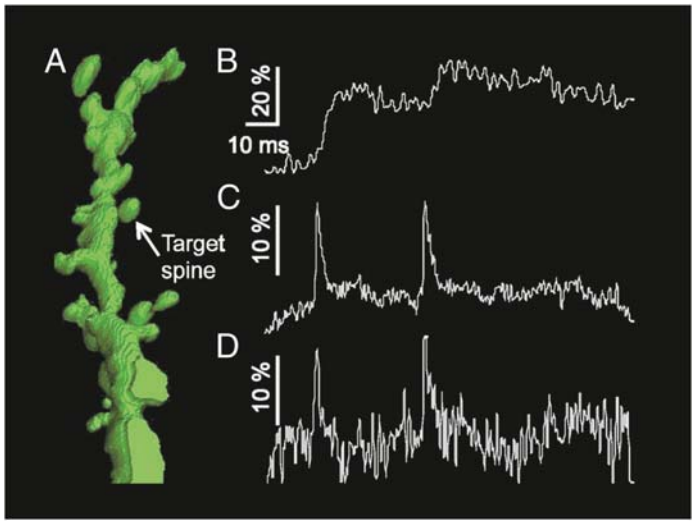

Figure 2.2: Simultaneous voltage and calcium imaging in a single dendritic spine. **A)** Reconstruction of the segment of proximal basal dendrite studied from a mouse acute cortical brain slice indicating the targeted spine. **B)** Calcium Green 1 Dextran fluorescence in response to two somatically initiated bAPs. **C)** Simultaneously recorded di-2-AN(F)EPPTEA VSD fluorescence transients. Both dyes are excited with the same two-photon laser tuned to 1020 nm. Waveforms are averages of 10 trials, with bleaching subtracted. **D)** Single-sweep VSD fluorescence. The vertical scale bars in B and C correspond to $\Delta F/F$.

edge of each dye spectrum. However, a range of wavelengths can be used for a given VSD without too much impact on $\Delta F/F$; because these dyes have greater fluorescence at 510 nm and a larger area is illuminated, the S:N in Figure 2.3 is improved compared with the two-photon records in Figure 2.1. This result occurs, because at these low-light levels, S:N is largely determined by the Poisson statistics of the emitted photons: sampling over an $\approx$100 μm^2 segment of dendrite membrane will deliver more photons than the $\approx$3 μm^2 surface of a typical single spine. Additional S:N considerations are described in subsection 2.2.5.

2.2.3 Spatiotemporal Mapping of Cardiac Tissue Physiology

We have already shown the efficacy of di-4-AN(F)EPPTEA to record APs from multiple subcellular sites on single cardiomyocytes [36]; in this section, we show the efficacy of other fluorinated VSDs in a whole-heart preparation. For illustrative purposes, three spectrally distinct dyes (blue, green, and red excitation wavelengths) were used in three common isolated whole-heart optical mapping applications: (i) sinus rhythm (di-4-AN(CF3)E(F)PPTEA), (ii) ventricular fibrillation (di-4-AN(F)EP(F)PTEA), and (iii) simultaneous voltage and $[Ca^{2+}]_i$ imaging (di-4-ANEQ(F)PTEA). Figure 2.4a shows a schematic of the imaging system used for all three applications [2, 37]. Figure 2.4b, Figure 2.4c, Figure 2.4d show AP recordings from the ventricles in initial experiments characterizing dyes di-4-AN(CF3)E(F)PPTEA, di-4-AN(F)EP(F)PTEA, and di-4-ANEQ(F)PTEA, respectively, in guinea pig hearts in sinus rhythm. Washout kinetics and photobleaching rate were also compared between spectrally similar di-4-ANEPPS

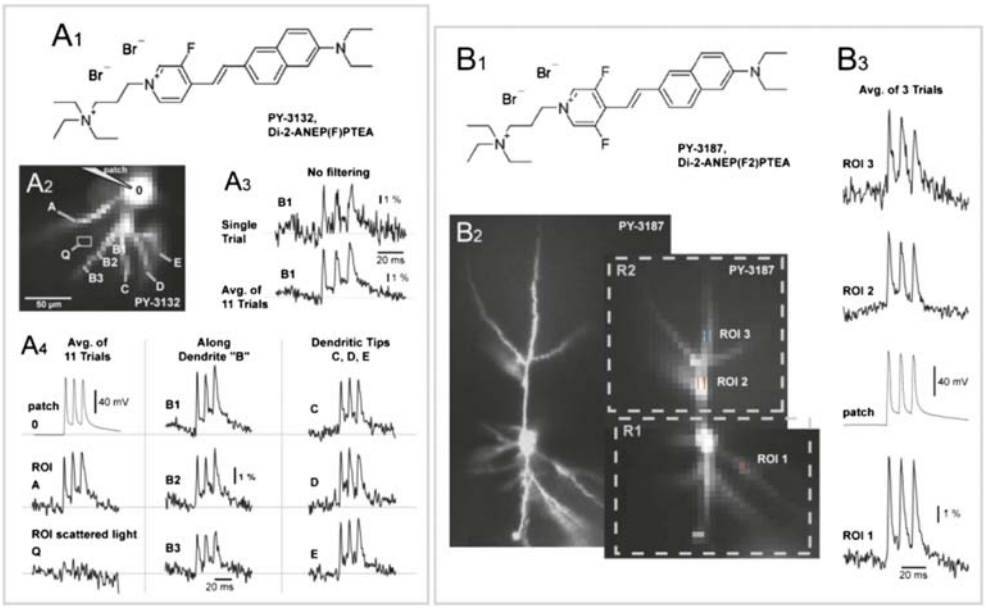

Figure 2.3: Simultaneous multisite recording of dendritic AP waveforms with two internally applied fluorinated dyes. **A1)** Structure of di-2-ANEP(F)PTEA. **A2)** Basal dendrites of a cortical pyramidal neuron injected with di-2-ANEP(F)PTEA and imaged with fast CCD camera (80 × 80 pixels; 2,000-Hz frame rate). **A3)** Brief current injections through a somatic patch pipette were used to trigger three APs. (Upper) An AP-associated optical signal obtained in a single recording sweep (no averaging) from the region of interest (ROI) indicated by B1. High-pass filter $\tau = 7$. Low-pass filter = 0. (Lower) Same as Upper, except that 11 sweeps were averaged. **(A4)** Multisite optical recordings of dendritic AP waveforms obtained from eight locations (ROIs) marked in A2. Each letter A–E marks a different basal branch. Three recordings (B1–B3) were obtained along the same branch. Three recordings (C–E) were obtained from the most distal dendritic segment (dendritic tip). The recording of the scattered light was obtained from region of interested Q. **B1)** The structure of di-2-ANEP(F2)PTEA. **B2)** The dendritic tree of a cortical pyramidal neuron injected with di-2-ANEP(F2)PTEA and imaged with the video camera used for IR differential interference contrast (DIC) video microscopy. Shown to the right are confocal images of the same neuron as seen by the fast CCD camera (80 × 80 pixels; 2000-Hz frame rate). The basal and apical portions of the dendritic tree were recorded in two positions (R1 and R2, respectively). **B3)** Current injections through a somatic patch pipette were used to trigger three APs. Optical recordings of dendritic AP waveforms obtained from three locations (ROIs) marked in B2. Each trace is a temporal average of three sweeps and spatial average of 3–4 pixels. The actual pixels used for spatial averaging are marked in B. High-pass filter $\tau = 7$. Low-pass filter = 500 Hz.

and di-4-AN(F)EP(F)PTEA (Figure 2.5). This finding shows the improved properties of these VSDs. Their $\Delta F/F$ and S:N are as good as standard VSDs used today [2, 38]. For di-4-ANEQ(F)PTEA (Figure 2.4d), the dye was also exposed to an excitation source for the low-affinity $[Ca^{2+}]_i$ reporter fura-4F (AM). A multiband emission filter collecting emission fluorescence for both fura-4F (AM) and di-4-ANEQ(F)PTEA was used (F3) (Figure 2.4a), showing that no cross-talk will occur in tissue additionally

loaded with fura-4F (AM).

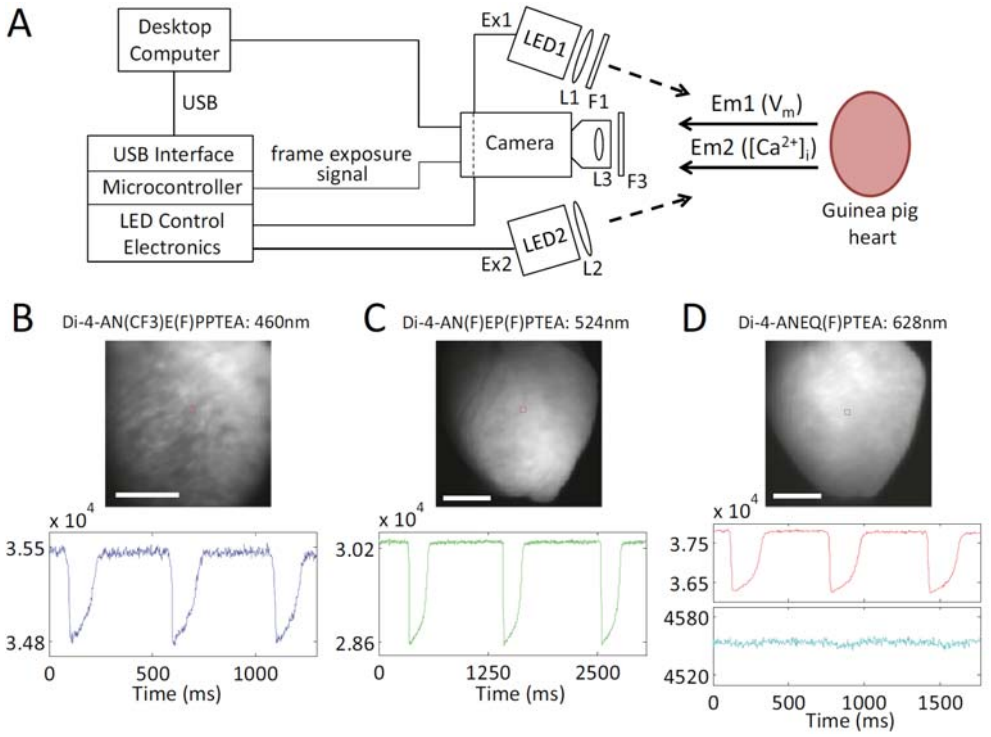

Figure 2.4: Whole-heart optical mapping of V_m. **A)** System layout with key components (section 2.4). Different light sources and optical filters were used for di-4-AN(CF3)E(F)PPTEA, di-4-AN(F)EP(F)PTEA, and di-4-ANEQ(F)PTEA. **B)** Raw (unfiltered) di-4-AN(CF3)E(F)PPTEA V_m signals, on a 16-bit scale, from a 4 ×4-pixel region of the heart in sinus rhythm. **C)** Raw (unfiltered) di-4-AN(F)EP(F)PTEA V_m signals, on a 16-bit scale, from a 4 ×4-pixel region of the heart in sinus rhythm. **D)** Raw (unfiltered) di-4-ANEQ(F)PTEA V_m signals, on a 16-bit scale, from a 4 ×4-pixel region of the heart in sinus rhythm exposed to excitation sources for both di-4-ANEQ(F)PTEA (Middle) and fura-4F AM (Bottom). Data were recorded before loading fura-4F AM as a control to show lack of cross-talk from the VSD. Scale bar: 5 mm.

Figure 2.6 shows activation waves on whole-heart ventricles (mostly left ventricle view) for the three VSDs. Figure 2.6a shows AP progression during sinus rhythm. Figure 2.6b shows sequential snapshots of chaotic electrical activity during ventricular fibrillation caused by bursts of rapid electrical pacing. Figure 2.6c shows simultaneous voltage and $[Ca^{2+}]_i$ imaging with the heart paced at the apex and coloaded with di-4-ANEQ(F)PTEA and fura-4F (AM), revealing the well-established delay between V_m and $[Ca^{2+}]_i$ peaks.

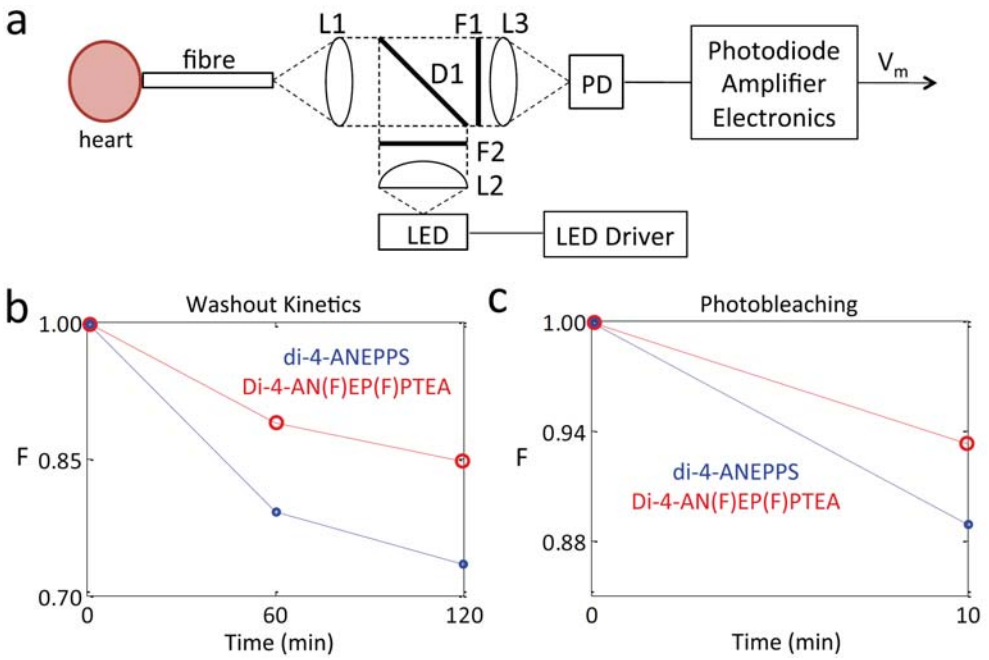

Figure 2.5: di-4-ANEPPS and di-4-AN(F)EP(F)PTEA washout kinetics and photobleaching rate. **A)** Schematic of the system used to compare washout kinetics and photobleaching rates in hearts loaded with either di-4-ANEPPS or di-4-AN(F)EP(F)PTEA. **B)** Normalized baseline total fluorescence of di-4-ANEPPS and di-4-AN (F)EP(F)PTEA in guinea pig hearts showing washout for three time points (details in the text). **C)** Normalized baseline total fluorescence of di-4-ANEPPS and di-4-AN(F)EP(F)PTEA in guinea pig hearts showing photobleaching after 10 min of continuous illumination (details in the text).

2.2.4 Random Access Two-Photon Recording of Electrical Activity in Cerebellum

We bathed a slice of cerebellum in di-4-AN(F)EPPTEA and were able to record spontaneous AP spikes from multiple Purkinje cells using two-photon excitation with a 1064-nm mode-locked fiber laser (Figure 2.7). This recording is achieved by rapidly positioning the laser excitation with an acousto-optic modulator to sample a patch of membrane from each cell in <100 μs; for recording from five cells as in Figure 2.7a, multiplexing permits a temporal resolution of ≈ 400 μs–sufficient to capture every spike. Figure 2.7b shows spontaneous activity recorded in this manner over 800 ms from the five neighboring cells, showing that spiking is not temporally correlated. Simultaneous optical and electrical recording from PC1 shows the high fidelity of the optical measurement. The expanded trace for PC5 in Figure 2.7b reveals the characteristic after hyperpolarization and shows the high temporal resolution of the random access microscope. Figure 2.7c, Figure 2.7d and Figure 2.7e show that the dye and the optical recording protocol do not produce any significant photodamage to the preparation.

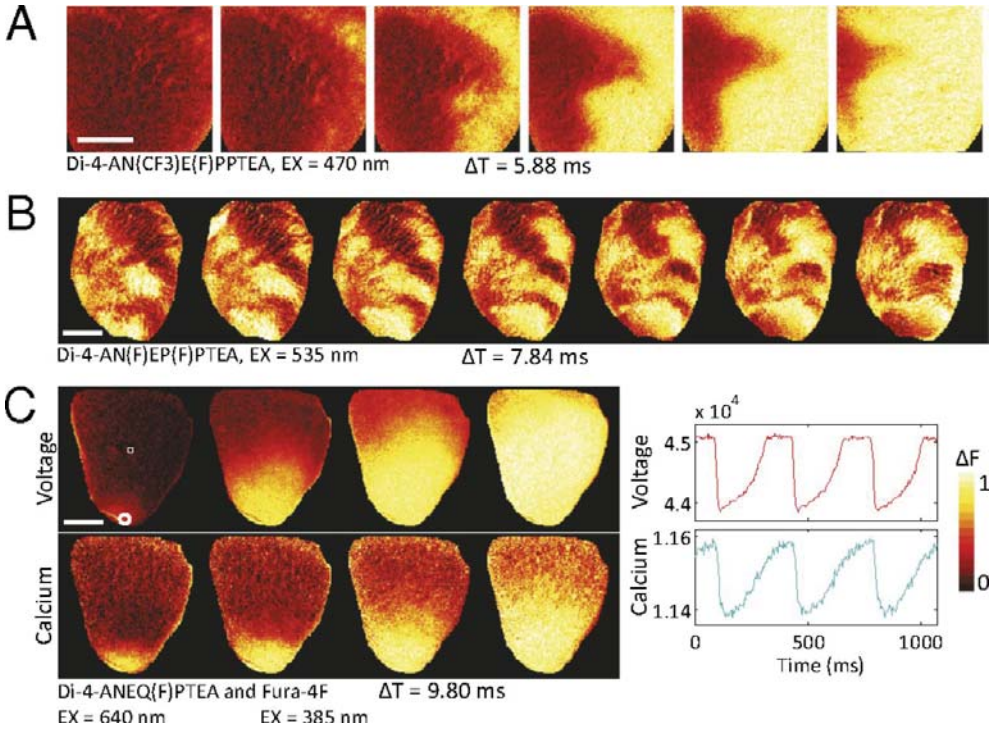

Figure 2.6: Guinea pig heart optical mapping. **A)** Normalized fluorescence intensity maps of V_m at six progressive time points during sinus rhythm. **B)** Normalized fluorescence intensity maps of V_m at seven progressive time points during ventricular fibrillation. **C)** Normalized fluorescence intensity maps of V_m and $[Ca^{2+}]_i$ at four progressive time points during local 4-Hz electrical stimulation of the apex (at the site of the white circle). Raw (unfiltered) V_m and $[Ca^{2+}]_i$ signals, on a 16-bit scale, are shown from a 4×4-pixel region on the ventricle. The color bar is shown at the bottom right for all normalized fluorescence intensity maps. Fluorescent indicators, excitation wavelengths, and time interval between frames are indicated below each image series. Scale bar: 5 mm.

2.2.5 Long-Wavelength Two-Photon Measurement of V_m in Cultured Hippocampal Neurons

Common near-infrared femtosecond laser sources used for two-photon microscopy have wavelength ranges from ca. 680 to 1080 nm. This range restricts the range of fluorescent probes for two-photon microscopy to chromophores with absorbance spectra below ≈540 nm. For hemicyanine VSDs, where red-edge excitation is optimal, the best dyes would have absorbance maxima at or below ≈470 nm, which is the case for di-3-ANEPPDHQ [15], di-2-AN(F)EPPTEA (Figure 2.1 and Figure 2.2), and di-4-AN(F)EPPTEA (Figure 2.7). However, this finding excludes most of the chromophores in Table 2.1 from two-photon applications. In particular, two-photon applications of a VSD combined with optogenetic manipulation or many $[Ca^{2+}]_i$ indicators would be facilitated if higher wavelength could be used for the VSD. We, therefore, decided to test several of the long-wavelength fluorinated VSDs by exciting them with light

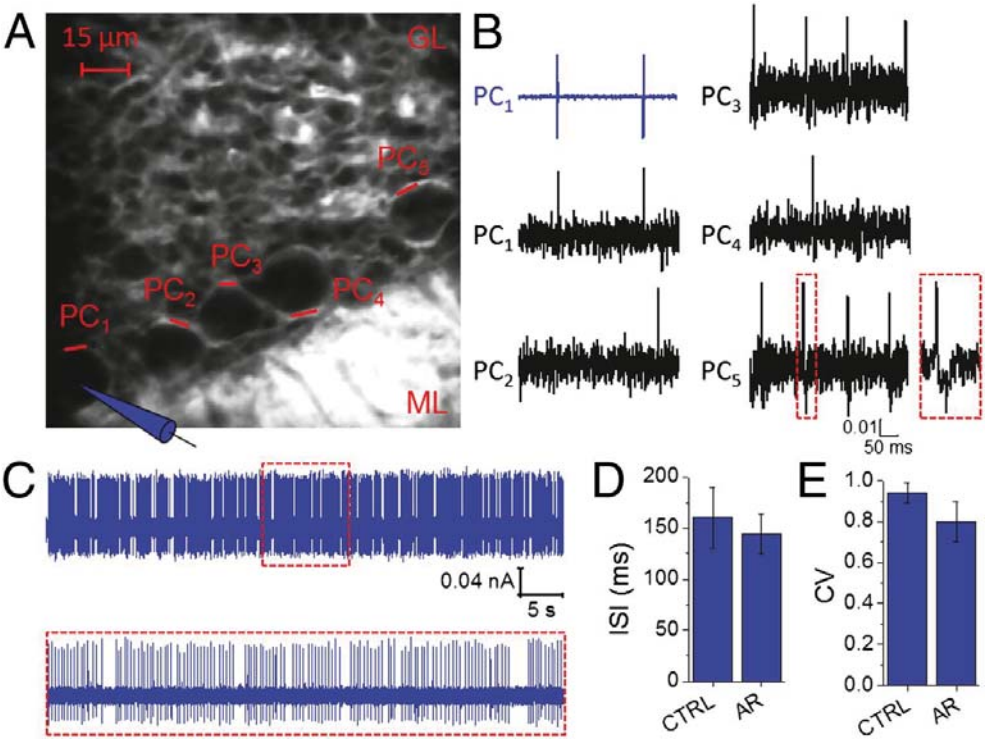

Figure 2.7: Real-time multicellular AP recording by random access multiphoton microscopy. **(A)** Two-photon fluorescence image (taken at a depth of 70 μm) of a parasagittal acute cerebellar slice stained with di-4-AN(F)EPPTEA. The molecular (ML) and granular (GL) layers are clearly distinguishable. The multiunit optical recording was carried out from the lines drawn (red) on the five Purkinje cells (PCs). The electrical activity (cell-attached recording) of PC1 was also monitored. **(B)** Real-time multiplexed optical recording of spontaneous activities from the five PCs (black traces) with a temporal resolution $\approx$400 μs. PC1 electrical activity measured by the electrode (blue trace) shows the reliability of the optical recording in spike detection. A simple spike in PC5 trace (red box) is shown at a higher temporal resolution, revealing the undershoot phase. **(C)** Electrical recording of spontaneous activity after the multiline scans session. A central region of the trace is expanded (6$\times$) in the dashed red box. **D** and **E)** The interspike interval (ISI) and the coefficient of variation (CV) measured before (CTRL) and after (AR) the optical recording session are not statistically different, indicating negligible photodamage induced by di-4-AN(F)EPPTEA.

in the range of 1100–1300 nm using a microscope in which the Ti-sapphire laser was coupled to an optical parametric oscillator.

We applied the VSDs externally to cultured dissociated hippocampal neurons to obtain a closer estimate of the intrinsic V_m sensitivity of the VSDs (Figure 2.8a), and in a first set of experiments, we acquired the fluorescence by rapid line scans along a short plasma membrane segment of a patch-clamped cell. The fluorescence responses to a 50-Hz train of square voltage-clamp hyperpolarizations were recorded. The excitation wavelength for each dye was chosen by finding the region of maximum slope on the red wing of its absorbance spectrum in dimethyl sulfoxide solution (all of the

dyes were highly soluble in this solvent); no additional attempt was made to find the wavelength for optimal $\Delta F/F$. Figure 2.8b shows the response of the five tested dyes. Although di-2-ANEP(F)PTEA and di-4-ANEQ(F)PTEA seem to be more sensitive than the long-wavelength nonfluorinated dye, di-2-ANEQPTEA, the differences were not statistically significant ($P = 0.23$, Kruskal-Wallis). However, under two-photon excitation, the effect of fluorination significantly improved photostability (Figure 2.8c) of di-2-ANEP(F)PTEA, di-2-ANEP(F2)PTEA, and di-4-ANEQ(F)PTEA (with $P < 0.0125$, Wilcoxon rank sum and Bonferroni criterion); it showed, on average, bleaching up to 11% compared with di-2-ANEQPTEA, which showed 32% after exposure to 2150 scans. Based on these results, we chose to test more di-2-ANEP(F)PTEA for single-sweep AP detection in a fixed spot illumination mode. With 20 mW at 1160 nm during brief 30-ms exposures, we could clearly resolve single APs (Figure 2.8d) without observing any increase in leak current, even after 20 repetitions (the fluorescence was corrected for ≈25% bleaching). By averaging the filtered optical signal from 20-well timed APs, we found a close match between the optical and patch-clamp recorded AP waveforms (Figure 2.8e), showing the linearity of the dye response. The results summarized in Figure 2.8f show that di-2-ANEP(F)PTEA had a V_m sensitivity of 14.6 ± 4.6%/100 mV (median ± SD); the S:N of the total fluorescence was 176 ± 82 (median ± SD). This finding enabled single-trial 90-mV AP-induced changes in the V_m to be detected with a S:N of 23.2 ± 5.0 (median ± SD) from a micrometer-sized spot under two-photon excitation. Although the wavelength dependence of the S:N for F has a generally negative slope, which would be expected for shot noise limited detection, S:N for $\Delta F/F$ has no obvious wavelength dependence; this result occurs, because as the wavelength increases, the $\Delta F/F$ becomes larger as the noise becomes relatively larger (of course, if there is enough laser power, it can be used to improve the S:N at the red edge of the VSD spectra). After pooling both the voltage step and AP datasets, we found that di-2-ANEP(F)PTEA was not only more photostable than di-2-ANEQPTEA but also, significantly more sensitive to the V_m ($P = 0.003$, Wilcoxon rank sum) with $\Delta F/F$ =12.4 ± 4.2%/100 mV (median ± SD) compared with 7.9 ± 1.0%/100 mV (median ± SD), respectively. The maximum $\Delta F/F$ observed for di-2-ANEP(F)PTEA was 21%/100 mV; the lower average $\Delta F/F$ and its variability can be attributed to fluorescence coming from internalized dye bound to intracellular membranes.

2.3 Discussion

The VSDs listed in Table 2.1 cover a broad range of wavelengths, with absorbance maxima of the membrane-bound dyes ranging from 400 to 553 nm and emission maxima ranging from 589 to 743 nm. For each VSD, red-edge excitation at about 60 nm above the absorbance maximum offers optimal $\Delta F/F$, but there is a broad-wavelength window over which the response is close to the maximum [7, 17, 29]. This window stretches the usable excitation range over which good sensitivity can be obtained with the new palette of VSDs from 440 to 670 nm (Figure 2.6). Additionally, the hemicyanines have the distinct advantage of large Stokes shifts. Although common cyanine and xanthene fluorescent dyes and typical fluorescent protein probes have Stokes shifts of 20–40 nm, hemicyanines have emission spectra that are shifted by ≈170 nm from their absorbance/excitation maxima (Table 2.1). Thus, a single excitation source can

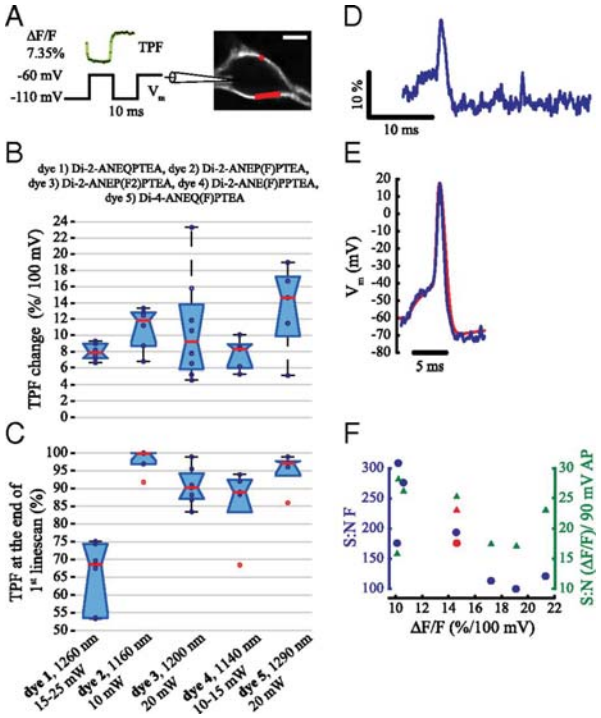

Figure 2.8: Characterization of long-wavelength VSDs with two-photon excited fluorescence on cultured hippocampal neurons. **A)** Example of a patch-clamped hippocampal cultured neuron stained with a VSD. Scale bar: 10 μm. Fluorescence measurements were done in both line scan mode at 3.5 KHz along the somatic membrane and fixed spot illumination mode with 20 KHz sampling (red marks). Screening of VSDs was done using line scans along the soma membrane during the multiple voltage-clamp stepping cycles. The optical trace (green) shows the average of 60 trials with 20 50-mV steps per trial using di-4-ANEQ(F)PTEA with 1290-nm excitation. **B)** Sensitivity of the dyes (notched box plot; red, median; dark blue circles, individual data points). The ordinate shows the percentage change in two-photon fluorescence (ΔF/F) per 100 mV voltage-clamp step and the abscissa common to C. **C)** Photostability of the VSDs after a 614-ms exposure to 2150 line scans at 3.5 KHz (notched box plot; red, median; dark blue circles, individual data points; red circles, outliers). In both B and C, each point in the two charts corresponds to a different cell. Laser powers used for each experiment were adjusted to produce approximately the same S:N for each VSD. Together with the wavelength and dye used, they are also listed along the abscissa. In another set of experiments, di-2-ANEP(F)PTEA was tested for single AP detection using a fixed spot illumination mode and 20-mW excitation at 1160 nm. **D)** Bleaching-corrected fluorescence signal sampled at 20 KHz and filtered with a five-point moving average (for presentation, trace has been inverted). **E)** Average of 20 AP fluorescent traces corrected for bleaching and filtered with a five-point moving average (blue) and average of 20 patch-clamp recorded APs (red). **F)** Summary of fluorescence S:N (blue filled circles) and 90-mV AP detection S:N (green triangles) of the 20 KHz sampled and five-point moving average-filtered optical trace and their medians (red). The S:N of detecting a 90-mV AP is the product of the ordinate S:N F and the abscissa ΔF/F $\times$ 0.9. Note that fluorescence decreased with depolarization, because the outer membrane leaflet was stained.

be used to excite both a hemicyanine VSD and a second fluorescent probe or sensor, and the responses readily separated with appropriate emission filters (Figure 2.2). Additionally, hemicyanine dyes have good two-photon cross-sections for excitation into their lowest-energy excited states, and therefore, the two-photon absorbance spectra are approximately at two times the wavelength of the one-photon spectra [39]. Although the range for two-photon excitation is shown from 1020 to 1290 nm in this work (Figure 2.2, Figure 2.7, Figure 2.8), the repertoire of VSDs in Table 2.1 should allow for effective two-photon voltage sensing at any wavelength between 900 and 1340 nm. Importantly, commercial Ti-sapphire laser systems are becoming available to cover the entire range from 680 to 1300 nm. Thus, the availability of the VSDs in Table 2.1 should allow superior flexibility in the design of experiments with various light sources and cell and tissue preparations and combined with other optical tools for manipulation and sensing of cell physiology.

The photostability of fluorescent probes can be a critical factor in their practical application when the duration of the event of interest or the copy number of fluorescent molecules is small, which would occur in subcellular microscopic measurements. This finding is because the noise in such measurements is dominated by the shot noise caused by the limited number of photons being detected. A dye with high photostability will produce more photons before it is bleached than a dye with low photostability, and therefore, the former can produce fluorescence with intrinsically better S:N. Although we do not present a systematic study of the effect of fluorination on photostability, which is beyond the scope of this work, there is ample precedent that fluorination is beneficial [32, 33]. We do show, in several practical tests for our fluorinated VSDs, that they show improved photostability and correspondingly, display little evidence for photodynamic damage to the specimen. Figure 2.1 shows that 40 160-ms exposure trials cause no deterioration in the optical signal obtained from a single dendritic spine. Figure 2.5 shows that di-4-ANEPPS bleaches almost two times as fast in a guinea pig heart as di-4-AN(F)EP(F)PTEA, which has nearly identical spectral properties. Similarly, for long-wavelength two-photon excitation, Figure 2.8c shows that the three fluorinated VSDs tested are three to six times more photostable than a long-wavelength nonfluorinated VSD. Additionally, Figure 2.2 and Figure 2.7 provide evidence that, under conditions of prolonged optical recording, these VSDs do not seem to change the electrophysiology properties of the biological substrate.

The application vignettes in Figure 2.2, Figure 2.6, Figure 2.7 and Figure 2.8 show the efficacy of the dyes for single cells in culture, externally and internally stained neurons in brain slices, and whole-heart preparations. Additionally, we have recently reported the ability of di-4-AN(F)EPPTEA to map subcellular AP properties in single cardiomyocytes [36]. These examples show the high sensitivity of the fluorinated VSDs in subcellular, single-cell, and tissue-level applications. They also show the efficacy of the dyes with both one- and two-photon excitation. Figure 2.2, Figure 2.6, Figure 2.7 and Figure 2.8 indicate that the voltage sensitivities of the fluorinated VSDs are comparable with and often exceed the sensitivities of the best conventional hemicyanines. The ability to choose from the large palette of VSDs listed in Figure 2.2, Figure 2.6, Figure 2.7 and Figure 2.8 assures that sensitivity and other properties (solubility, photostability, toxicity, excitation wavelength, emission wavelength, etc.) can be optimized to meet the varying demands of a large range of optical electrophysiology experiments.

2.4 Materials and Methods

The detailed preparation and characterization of di-4-AN(F)EPPTEA and di-2-AN(F)-EPPTEA have been reported [29, 36]. The synthetic procedures for the other VSDs in Table 2.1 all involve the same aldol coupling chemistry used for the published syntheses. Further details on the dye spectral measurements, biological preparations, electrophysiological recording methods, and fluorescence imaging setups (Figure 2.9) are detailed below.

Absorption and Emission Spectra of VSDs Bound to Lipid Vesicle Membranes

A stock solution of lipid vesicles was prepared by sonicating soybean phosphatidylcholine in PBS buffer (20 mg/mL) to clarity with an ultrasonic cleaner (Model G112SP1T; Laboratory Supplies). Absorption spectra of VSDs bound to lipid vesicle membranes were measured in PBS buffer containing 2 mg/mL lipid on a Shimadazu UV-Visible spectrophotometer (Model UV-1601PC). Corrected emission spectra were obtained with a HORIBA Jobin Yvon fluorescence spectrometer (Model FL3-211).

Spine Voltage and Calcium Recordings in Acute Cortical Brain Slice by Two-Photon Excited Fluorescence

Acute coronal brains slices from prefrontal cortex of mice ages P23 to P28 were prepared as described previously [29, 40]. Loading of VSD generally requires whole-cell patching each neuron two times, called repatching, and we followed the same techniques that we have used and published [29, 40]. Briefly, the first patch pipette (typically 8–10 MΩ) is filled with a small amount of dye-free intracellular solution at the tip followed by a high concentration of VSD dissolved in normal intracellular solution. Here, in addition to the VSD, Calcium Green 1 Dextran (3000 MW) was added at ≈1 mM concentration. After the dye fluorescence fills the soma, the patch pipette is withdrawn, and the dyes are allowed to diffuse into the dendrites. Finally, the neuron was repatched with intracellular solution containing 1 mM Calcium Green 1 Dextran (pipette resistance is typically 6.5–8 MΩ). APs could be evoked through current injection. Calcium signals in spines were not visible immediately on repatching, and instead, they became visible after ≈10 min. Single-voxel recordings were made from targeted spines using 1020-nm excitation as previously described [29, 40] using a custom two-photon microscope. The microscope configuration that allows for simultaneous voltage and $[Ca^{2+}]_i$ recording is shown in Figure 2.9.

One-Photon Excited Fluorescence Back-Propagating AP Recording from Distal Dendritic Segments

The experiments carried out with the VSDs used a very similar apparatus and experimental preparation as reported previously [41]. Sprague-Dawley rats (postnatal days 21–33) were anesthetized with halothane and decapitated, and the brain was removed with the head immersed in ice-cold artificial cerebrospinal fluid according to an animal protocol approved by the Center for Laboratory Animal Care, University of Connecticut. Brain slices (300 μm) were cut from frontal lobes in the coronal plane. Artificial cerebrospinal fluid contained (in mM) 125 NaCl, 26 NaHCO3, 10 glucose, 2.3 KCl, 1.26 KH2PO4, 2 CaCl2, and 2 MgSO4 (pH 7.4). Whole-cell recordings were made that visually identified layer V pyramidal neurons. Intracellular solution contained (in mM)

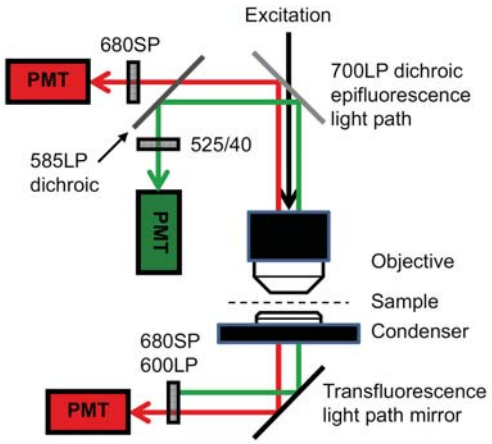

Figure 2.9: Microscopy and data analysis for simultaneous two-photon voltage and calcium imaging. Cartoon diagram of the microscope built on a Zeiss Axioskop 2FS MOT with a Zeiss 40×, 1.0 N.A. objective and a Zeiss 1.2 N.A. water condenser. Interference filter and dichroic mirror wavelengths are shown for the custom epi- and transfluorescence detection pathways. Red VSD fluorescence is collected in both pathways with two photomultiplier tubes (PMTs) combined into one channel using a single current-sensitive amplifier, whereas the green Ca^{2+} dye fluorescence is collected only in the epifluorescence pathway. The laser beam is raster-scanned with a pair of galvo mirrors (Cambridge Instruments, Inc.).

135 K-gluconate, 2 MgCl2, 3 Na2-ATP, 10 Na2-phosphocreatine, 0.3 Na2-GTP, and 10 HEPES (pH 7.3; adjusted with KOH). VSD injections were described previously [42]. Each dye was dissolved in the intracellular solution (400–600 μM) and loaded into neurons through whole-cell pipettes (30–45 min). Loading pipettes were then pulled out (outside-out patch), and the loaded neurons were incubated at room temperature for 1–2 h. Before imaging, neurons were repatched with dye-free electrodes. Multisite dendritic imaging was performed on an Olympus BX51WI microscope equipped with 40× objective, two camera ports, and a low-ripple Xenon arc lamp (OptiQuip) for epi-illumination. Fluorescence signals were recorded optically (excitation=510 ± 40 nm, dichroic=570 nm, emission >610 nm) using a 2-kHz frame rate (80 × 80 pixels; NeuroCCD; RedShirtImaging) camera. A spike-triggered averaging routine available in the data acquisition software, Neuroplex (RedShirtImaging), was used to improve the signal-to-noise ratio of VSD measurements. Each trace in Figure 2.3 is a spatial average of 3–4 pixels. The actual pixels used for spatial averaging are marked by vertical dashes in Figure 2.3b.

Isolated Langendorff-Perfused Guinea Pig Whole Heart

Hearts were isolated from female guinea pigs (300–500 g) after cervical dislocation in accordance with Schedule 1 of the United Kingdom Home Office Animals (Scientific Procedures) Act of 1986 and swiftly connected to a Langendorff perfusion setup [n = 2 for di-4-AN(CF3)E(F)PPTEA; n = 2 for di-4-AN(F)EP(F)PTEA; n = 2 for di-4-ANEQ(F)PTEA]. Hearts were perfused at a constant rate of 8 mL/min with a modified Krebs-Henseleit solution (containing, in mM, 125 NaCl, 1.8 CaCl2, 5.4 KCl 5.4, 25 NaHCO3, 1.2 NaH2PO4H2O, 1 MgCl2, 5.5 D-glucose, 0.2 probenecid;

Sigma-Aldrich) gassed with 95% O2/5% CO2 to maintain a pH of 7.4. Fluorescent dyes were injected into the aortic cannula for coronary perfusion. For V_m imaging, the heart was loaded with dye by delivering, without recirculation, a 15-μL bolus of di-4-AN(CF3)E(F)PPTEA stock solution (16 mg/mL in pure ethanol), di-4-AN(F) EP(F)PTEA stock solution (17 mg/mL in pure ethanol), or di-4-ANEQ(F)PTEA stock solution (17 mg/mL in pure ethanol) applied slowly over 2 min (i.e., diluted in 16 mL perfusate); 2 μL Pluronic F-127 (Life Technologies) were added to each bolus. For $[Ca^{2+}]_i$ imaging, hearts were dye-loaded by recirculating 100 mL perfusate containing 2.5 μmol/L fura-4F AM (Life Technologies) for 30 min. For suppression of motion, excitation-contraction was uncoupled with blebbistatin (Sigma-Aldrich) at 10 μmol/L [43]. All whole-heart experiments were conducted at 36 $\pm$ 1 °C.

Whole-Heart Optical Mapping System
The system implemented here was a modification of a four-parameter imaging system described elsewhere [37], where detailed circuit diagrams and software code are provided. Provided below is a brief description of the setup shown in Figure 2.4a.

Excitation of di-4-AN(CF3)E(F)PPTEA was done using:

- LED1: CBT-90-B (peak power output = 53 W, peak wavelength = 460 nm; Luminus Devices).
- L1: plano-convex lens (LA1951; Thorlabs).
- F1: D470/20X (Chroma Technology).

Excitation of di-4-AN(F)EP(F)PTEA was done using:

- LED1: CBT-90-G (peak power output = 58 W, peak wavelength = 524 nm; Luminus Devices).
- L1: plano-convex lens (LA1951; Thorlabs).
- F1: D535/25X (Chroma Technology).

Excitation of di-4-ANEQ(F)PTEA was done using:

- LED1: CBT-90-R (peak power output = 32 W, peak wavelength = 628 nm; Luminus Devices).
- L1: plano-convex lens (LA1951; Thorlabs).
- F1: D640/20X (Chroma Technology).

Excitation of fura-4F AM was done using:

- LED2: NCSU034A (peak power output = 400 mW, peak wavelength = 385 nm; Nichia).
- L2: plano-convex lens (LA1951; Thorlabs).

Fluorescence emission was passed through (i) a single-band emission filter F3: BLP01-561R-25 (Semrock) for di-4-AN(CF3)E(F)PPTEA and di-4-AN(F)EP(F)PTEA or (ii) a custom (now off the shelf) multiband emission filter F3: ET525/50-800/200M (Chroma Technology) for di-4-ANEQ(F)PTEA. Emission was then collected through L3: a fast camera-suitable lens (f/# 0.95, DO-1795; Navitar). Fluorescence images were taken with a highspeed EMCCD camera (Cascade 128+; Photometrics). The resolution was 128 × 128 pixels, and the frame rate was 511 fps. Acquisition software QCapture Pro-6.0 (QImaging), which came with the camera system, was used to configure the camera and acquire images. During simultaneous imaging of V_m and $[Ca^{2+}]_i$ [i.e., di-4-ANEQ(F)PTEA and fura-4F AM], a microcontroller-based interface synchronized excitation light switching with EMCCD camera frame exposures. The LEDs were controlled with a custom-built high-power LED driver circuit (6). An eight-processor microcontroller (Propeller chip; Parallax) was used to control and coordinate all major components of the setup. Communication with a standard desktop

computer was achieved with a USB interface module (UM245R; Future Technology Devices International). Custom software written in MATLAB (MathWorks) was used to communicate with the microcontroller and perform image processing. All electronic components were acquired from major electronic components distributors (Digi-Key Corp). Whole hearts were electrically stimulated with biphasic pulses having an amplitude of ≈5 V and duration of 2 ms generated by a custom-built stimulator. A bipolar concentric stimulation electrode was used (Lohmann). To generate ventricular fibrillation from Figure 2.4b, burst pacing at cycle lengths of 30–50ms was performed for ≈1 s (7); 4-Hz pacing was performed at the apex for Figure 2.4c.

Two-Photon Recording of Spontaneous Activity from Several Purkinje Cells in a Cerebellar Brain Slice

Acute cerebellar slices (200- to 250-μm thick) were obtained from 14- to 18-day-old Wistar Han rats. The dye loading was performed by incubating a slice for ≈30 min at a temperature of ≈30 °C in 1 mL oxygenated Krebs solution containing 0.05 mg di-4-AN(F)EPPTEA dye. The stained slice was gently positioned on the recording chamber and continuously perfused during the recording session. Measurements were performed at room temperature. During optical recordings, the excitation was provided by a high-power, passively mode-locked fiber laser operating in the 1064-nm spectral range (200-fs-width pulses at 80-MHz repetition rate). The scanning head was developed by using an acousto-optical deflection (AOD) system comprised of two AODs crossed at 90°. To compensate for the larger dispersion caused by two crossed AODs, we use an acousto-optic modulator placed at 45° with respect to the two axes of the AODs. A water immersion objective (40×, N.A. 0.8; Olympus) was used to focus the excitation light in the tissue. The fluorescence signal was collected in the backward direction by the excitation objective and in the forward direction using a condenser lens (N.A. 1.4; Olympus). The fluorescence signal was detected by two independent GaAsP photomultiplier modules (H7422; Hamamatsu). Emission filters of 655 ± 20 nm (Semrock) were used. The AODs scanning system is capable of commutating between two positions of the focal plane in ≈4 μs. In a typical measurement, we probe three to six different neurons. The length of the scanned lines is ≈5 μm, with integration time per membrane ranges from 50 to 100 μs.

Long-Wavelength Two-Photon VSD Measurements

Cell cultures were obtained from hippocampi of mouse E18 embryos by 0.25% tripsin (Invitrogen) digestion in HBSS/Hepes for 20 min at 37 °C. Tissue was washed three times in HBSS/Hepes and triturated with a fire-polished glass pipette. Dissociated neurons were plated at a density of 25000 cells/well on top of a layer of rat glial cells grown at a density of 37500 cells/well on 18-mm glass coverslips (Menzel) in 12-well plates. Cells were grown in Neurobasal medium (Invitrogen) supplemented with B27 (Invitrogen), 18 mM Hepes, 0.5 mM Glutamax (Invitrogen), and penicillin/streptomycin (Invitrogen). One-half the medium was replaced one time per week. Electrodes were pulled from borosilicate-glass capillaries with a 4- to 5-MΩ series resistance with the following intracellular and extracellular medium. Intracellular medium (in mM): 125 K-Gluconate, 10 NaCl, 4.6 MgCl, 4 K2ATP, 15 creatine phosphate, and 2.4 mg/50 mL phosphocreatine kinase (pH was adjusted with KOH to 7.3, and final osmolarity was 300 mOsm). External medium (in mM): 10 HEPES, 10 D-glucose, 140 NaCl, 2.4 KCl, 2 CaCl2, and 4 MgCl2 (pH was adjusted with NaOH to 7.3, and final osmola-

rity was 300 mOsm). VSD membrane potential sensitivity screening was done under voltage clamp using a HEKA EPC-8 patch-clamp amplifier by stepping the membrane potential between 110 and 60 mV every 10 ms to avoid escape from voltage clamp and rebound spiking. Pipette serial resistance was left uncompensated; however, the cell charging time constant was much faster than the membrane potential step duration. In single-shot AP detection experiments, APs were induced reliably in current clamp mode by a brief current pulse, and experiments were valid if the AP shape or height did not change significantly. Bridge balancing was done offline using a custom written Matlab script (Matlab R2008a; MathWorks). All membrane potential recordings were corrected for junction potential. VSDs were stored in ethanol at 20 °C, and on the day of experiment, they were diluted in extracellular solution by first letting the EtOH evaporate and then adding the extracellular solution to obtain a dye concentration of 4 μM. Culture coverslips were placed under the microscope with 300 μL extracellular solution, and cells were patch-clamped, after which 200 μL extracellular solution containing the VSDs at 4 μM were added in the case of line scan experiments and 600 μL extracellular solution were added in the case of single-shot AP detection experiments. Experiments were performed with a commercial two-photon laser-scanning microscope (TrimScope; LaVision BioTec GmbH). The light source was an optical parametric oscillator (Mira-OPO; APE) pumped at 810 nm by a mode-locked Ti:Sapphire laser (Ultra II; Coherent Chameleon). The light was focused onto the sample using a 20×, 0.95 N.A. water-dipping objective (XLUMPFL-IR; Olympus), and fluorescence was separated from the excitation by a custom dichroic (T800lpxrxt; Chroma) and detected using a GaAsP high-sensitivity photomultiplier tube (H7422-40; Hamamatsu). Excitation duration was controlled using a fast mechanical shutter (VS14S2ZMO; Uniblitz). Linescan triggers were aligned to electrophysiology by recording both variables using a separate DAQ board (NI USB-6221). Imaging was started <2 min after dye application to avoid internalization by the cells, and therefore, most of the two-photon excited fluorescence originated from dye bound to the outer membrane leaflet. This approach allowed a better estimate of the dyes intrinsic membrane potential sensitivity. For dye screening, the membrane potential was switched between 110 and 60 mV every 10 ms, line scans were done at 3500 Hz along the soma membrane, where two-photon fluorescence was maximal because of the parallel orientation of the dyes transition dipole moment to the linearly polarized excitation laser. The laser powers used and the wavelengths were adjusted as shown in Figure 2.8c, and therefore, there were no significant differences between the S:N of the different dyes (P = 0.9, Kruskal-Wallis). For single-shot AP measurements, the beam was parked on the soma membrane where fluorescence was highest because of favorable dye orientation, and fluorescence was sampled at 20 KHz during 20 30-ms exposures repeated every 2 s. Analysis was carried out in Matlab (Matlab R2008a; MathWorks).

References

1. Canepari, M. & Zecevic, D. *Membrane potential imaging in the nervous system: methods and applications* (Springer Science & Business Media, 2010).
2. Herron, T. J., Lee, P. & Jalife, J. Optical imaging of voltage and calcium in cardiac cells & tissues. *Circulation research* **110,** 609–623 (2012).
3. Loew, L. M., Bonneville, G. W. & Surow, J. Charge shift optical probes of membrane potential. Theory. *Biochemistry* **17,** 4065–4071 (1978).

4. Loew, L. M., Simpson, L., Hassner, A. & Alexanian, V. An unexpected blue shift caused by differential solvation of a chromophore oriented in a lipid bilayer. *Journal of the American Chemical Society* **101,** 5439–5440 (1979).
5. Loew, L., Scully, S., Simpson, L. & Waggoner, A. Evidence for a charge-shift electrochromic mechanism in a probe of membrane potential. *Nature* **281,** 497–499 (1979).
6. Loew, L. M. *et al.* A naphthyl analog of the aminostyryl pyridinium class of potentiometric membrane dyes shows consistent sensitivity in a variety of tissue, cell, and model membrane preparations. *Journal of Membrane Biology* **130,** 1–10 (1992).
7. Fluhler, E., Burnham, V. G. & Loew, L. M. Spectra, membrane binding, and potentiometric responses of new charge shift probes. *Biochemistry* **24,** 5749–5755 (1985).
8. Bedlack, R., Loew, L., *et al.* Localized membrane depolarizations and localized calcium influx during electric field-guided neurite growth. *Neuron* **9,** 393–403 (1992).
9. Canepari, M., Willadt, S., Zecevic, D. & Vogt, K. E. Imaging inhibitory synaptic potentials using voltage sensitive dyes. *Biophysical journal* **98,** 2032–2040 (2010).
10. Zecevic, D. Multiple spike-initiation zones in single neurons revealed by voltage-sensitve dyes. *Nature* **381,** 322 (1996).
11. Grinvald, A., Frostig, R., Lieke, E. & Hildesheim, R. Optical imaging of neuronal activity. *Physiological reviews* **68,** 1285–1366 (1988).
12. Fromherz, P., Hübener, G., Kuhn, B. & Hinner, M. J. ANNINE-6plus, a voltage-sensitive dye with good solubility, strong membrane binding and high sensitivity. *European Biophysics Journal* **37,** 509–514 (2008).
13. Kuhn, B., Fromherz, P. & Denk, W. High sensitivity of Stark-shift voltage-sensing dyes by one-or two-photon excitation near the red spectral edge. *Biophysical journal* **87,** 631–639 (2004).
14. Obaid, A., Loew, L., Wuskell, J. & Salzberg, B. Novel naphthylstyryl-pyridinium potentiometric dyes offer advantages for neural network analysis. *Journal of neuroscience methods* **134,** 179–190 (2004).
15. Fisher, J. A. *et al.* Two-photon excitation of potentiometric probes enables optical recording of action potentials from mammalian nerve terminals in situ. *Journal of neurophysiology* **99,** 1545–1553 (2008).
16. Matiukas, A. *et al.* Near-infrared voltage-sensitive fluorescent dyes optimized for optical mapping in blood-perfused myocardium. *Heart Rhythm* **4,** 1441–1451 (2007).
17. Wuskell, J. P. *et al.* Synthesis, spectra, delivery and potentiometric responses of new styryl dyes with extended spectral ranges. *Journal of neuroscience methods* **151,** 200–215 (2006).
18. Bradley, J., Luo, R., Otis, T. S. & DiGregorio, D. A. Submillisecond optical reporting of membrane potential in situ using a neuronal tracer dye. *Journal of Neuroscience* **29,** 9197–9209 (2009).
19. Ehrenberg, B., Montana, V., Wei, M., Wuskell, J. & Loew, L. Membrane potential can be determined in individual cells from the nernstian distribution of cationic dyes. *Biophysical journal* **53,** 785–794 (1988).
20. Gonzalez, J. E. & Tsien, R. Y. Improved indicators of cell membrane potential that use fluorescence resonance energy transfer. *Chemistry & biology* **4,** 269–277 (1997).
21. Shoham, D. *et al.* Imaging cortical dynamics at high spatial and temporal resolution with novel blue voltage-sensitive dyes. *Neuron* **24,** 791–802 (1999).
22. Miller, E. W. *et al.* Optically monitoring voltage in neurons by photo-induced electron transfer through molecular wires. *Proceedings of the National Academy of Sciences* **109,** 2114–2119 (2012).
23. Akemann, W., Mutoh, H., Perron, A., Rossier, J. & Knöpfel, T. Imaging brain electric signals with genetically targeted voltage-sensitive fluorescent proteins. *Nature methods* **7,** 643–649 (2010).
24. Jin, L. *et al.* Single action potentials and subthreshold electrical events imaged in neurons with a fluorescent protein voltage probe. *Neuron* **75,** 779–785 (2012).

25. Tsutsui, H., Karasawa, S., Okamura, Y. & Miyawaki, A. Improving membrane voltage measurements using FRET with new fluorescent proteins. *Nature methods* **5,** 683 (2008).

26. Kralj, J. M., Douglass, A. D., Hochbaum, D. R., Maclaurin, D. & Cohen, A. E. Optical recording of action potentials in mammalian neurons using a microbial rhodopsin. *Nature methods* **9,** 90–95 (2012).

27. Fedorov, V. V. *et al.* Anatomic Localization and Autonomic Modulation of Atrioventricular Junctional Rhythm in Failing Human HeartsClinical Perspective. *Circulation: Arrhythmia and Electrophysiology* **4,** 515–525 (2011).

28. Fedorov, V. V. *et al.* Optical mapping of the isolated coronary-perfused human sinus node. *Journal of the American College of Cardiology* **56,** 1386–1394 (2010).

29. Acker, C. D., Yan, P. & Loew, L. M. Single-voxel recording of voltage transients in dendritic spines. *Biophysical journal* **101,** L11–L13 (2011).

30. Holthoff, K., Zecevic, D. & Konnerth, A. Rapid time course of action potentials in spines and remote dendrites of mouse visual cortex neurons. *The Journal of physiology* **588,** 1085–1096 (2010).

31. Palmer, L. M. & Stuart, G. J. Membrane potential changes in dendritic spines during action potentials and synaptic input. *Journal of Neuroscience* **29,** 6897–6903 (2009).

32. Renikuntla, B. R., Rose, H. C., Eldo, J., Waggoner, A. S. & Armitage, B. A. Improved photostability and fluorescence properties through polyfluorination of a cyanine dye. *Organic letters* **6,** 909–912 (2004).

33. Sun, W.-C., Gee, K. R. & Haugland, R. P. Synthesis of novel fluorinated coumarins: Excellent UV-light excitable fluorescent dyes. *Bioorganic & medicinal chemistry letters* **8,** 3107–3110 (1998).

34. Loew, L. & Simpson, L. Charge-shift probes of membrane potential: a probable electrochromic mechanism for p-aminostyrylpyridinium probes on a hemispherical lipid bilayer. *Biophysical journal* **34,** 353–365 (1981).

35. Teisseyre, T. Z. *et al.* Nonlinear optical potentiometric dyes optimized for imaging with 1064-nm light. *Journal of biomedical optics* **12,** 044001–044001 (2007).

36. Sacconi, L. *et al.* Action potential propagation in transverse-axial tubular system is impaired in heart failure. *Proceedings of the National Academy of Sciences* **109,** 5815–5819 (2012).

37. Lee, P. *et al.* Single-sensor system for spatially resolved, continuous, and multiparametric optical mapping of cardiac tissue. *Heart Rhythm* **8,** 1482–1491 (2011).

38. Entcheva, E. & Bien, H. Macroscopic optical mapping of excitation in cardiac cell networks with ultra-high spatiotemporal resolution. *Progress in biophysics and molecular biology* **92,** 232–257 (2006).

39. Fisher, J. A., Salzberg, B. M. & Yodh, A. G. Near infrared two-photon excitation cross-sections of voltage-sensitive dyes. *Journal of neuroscience methods* **148,** 94–102 (2005).

40. Acker, C. D. & Loew, L. M. Characterization of voltage-sensitive dyes in living cells using two-photon excitation. *Chemical Neurobiology: Methods and Protocols,* 147–160 (2013).

41. Zhou, W.-L. & Antic, S. D. Rapid dopaminergic and GABAergic modulation of calcium and voltage transients in dendrites of prefrontal cortex pyramidal neurons. *The Journal of physiology* **590,** 3891–3911 (2012).

42. Antic, S. D. Action potentials in basal and oblique dendrites of rat neocortical pyramidal neurons. *The Journal of physiology* **550,** 35–50 (2003).

43. Fedorov, V. V. *et al.* Application of blebbistatin as an excitation–contraction uncoupler for electrophysiologic study of rat and rabbit hearts. *Heart rhythm* **4,** 619–626 (2007).